

Molecular dynamics simulation and continuum modeling of straight-chain aggregate sintering: Development of a phenomenological scaling law

T. Hawa and M. R. Zachariah*

Department of Mechanical Engineering and Department of Chemistry and Biochemistry, University of Maryland, College Park, Maryland 20742, USA

and National Institute of Standards and Technology, Gaithersburg, Maryland 20899-1070, USA

(Received 8 January 2007; revised manuscript received 16 April 2007; published 8 August 2007)

Atomistic molecular dynamics simulation and a simple continuum viscous flow model are employed to investigate the sintering of straight-chain nanoparticle aggregates. The results are used to develop a phenomenological sintering scaling law. The chain aggregates investigated consist of up to 80 primary particles of silicon, with primary particles of 2.5–7 nm in diameter. We found that sintering of chain aggregates consists of three steps. In step (a), reaction between particles to minimize surface defects and development of a cylindrical like shape comprised an induction period. Step (b) consisted of contraction of the cylinder, which actually consisted of two contraction stages. The first stage was the local contraction stage where sintering occurs only at the ends of the particle chain, and the second stage involved the global contraction. The last step was the nominal sintering process from an oval to spherical shape. As expected, sintering time increases with increasing chain length, with the exception that very long chains fragmented. The sintering times normalized by the primary particle diameter showed a universal relationship which only depends on chain length. These results were found to be consistent with a mathematical model we develop based on continuum viscous flow. The model was able to predict the sintering time in excellent agreement with results obtained from molecular dynamics simulation for any chain length and any primary particle size for straight nanoparticle chain aggregates. The results for sintering times for aggregate chains could be summarized with a power law modification of the Frenkel viscous flow equation, to include a dependence on the number of particle connections in a chain aggregate: $t = t_{\text{Frenkel}}^* (N-1)^{0.68}$.

DOI: 10.1103/PhysRevB.76.054109

PACS number(s): 61.46.Df

I. INTRODUCTION

Nanoparticles are of substantial interest as fundamental building blocks for nanostructures and associated devices.^{1,2} These may be single particles of size up to 100 nm or primary particles composing large aggregates or agglomerates. At this length scale, the particle melting point decreases and optical and chemical properties change relative to bulk materials.^{3–7} Thus, control of particle morphology is critically important to create or preserve a desired material property.

For large scale production or for ultraclean materials, aerosol methods (i.e., gas phase production) are generally the method of choice.^{8–11} Aerosol synthesis, however, typically results in highly aggregated structures. In some cases this is a desired morphology, while in other cases it is desired to avoid agglomeration. Since during particle formation coagulation and sintering are occurring simultaneously, the eventual aggregate structure is a competition between these two effects.⁹ The size of the spherical primary particles and the growth of agglomerates are determined by the rate of collision and subsequent sintering of particles. Therefore, particle morphology and size can be controlled by either modifying the characteristic coalescence or collision time. To understand the dynamics, it would be useful to understand how aggregates sinter.

For two bare particles of equivalent size, the characteristic coalescence time is obtained from either phenomenological solid state diffusion¹⁰ or viscous flow¹¹ models, depending on the controlling mechanism. In prior studies, we investi-

gated using molecular dynamics simulation the characteristic coalescence times for binary particles and compared them with phenomenological models.¹² We also investigated surface (hydrogen) passivation on the sintering and morphology of silicon nanoparticles and presented a phenomenological model to describe the dynamics during the coalescence of these coated particles.¹³ Our model, extended from the Frenkel model, was able to describe the entire coalescence process. More recently, we focused on understanding the coalescence mechanisms of unequal sized nanoparticles.¹⁴ We found that the Koch-Friedlander model accurately predicted the coalescence time of two unequal sized particles when benchmarked against the molecular dynamics (MD) simulation results. We also found that the characteristic coalescence times are independent of the volume ratio of the coalescing partners. However, all these studies focus on the kinetics of binary pairs of particles.

Several researchers have approached the problem of aggregate sintering using Monte Carlo or other Brownian dynamics approaches. A Monte Carlo grid-base model in two dimensions has been developed,¹⁵ where the sintering model assumes that particles take random walks on the surface of the aggregate. Recently, Kulkarni and Biswas introduced a simple Brownian dynamics simulation approach to understand the evolution of morphology of a sintering deposit.¹⁶ Their sintering model conserves mass and computes the associated surface area based on a sintering model proposed by Friedlander and Wu (1994).¹⁰ However, during sintering their particles retain a single point contact without merging with each other and assume a radius shrinkage for one par-

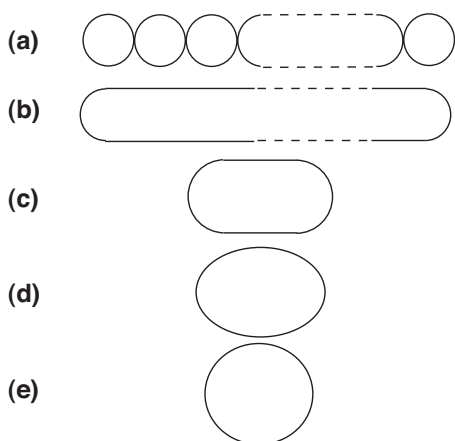


FIG. 1. Schematic representation of the sintering of a particle chain aggregate.

ticle and growth for the other as a means to conserve mass. Schmid *et al.* considered that the sintering particles are merging and the remaining parts of the two particles maintain a spherical shape, much like Frenkel's model.¹⁷

In all the approaches above, the aggregate sintering was simulated by making assumptions as to how sintering would occur in an aggregate, and then applying a standard sintering approach to map the evolution of the morphology.

Our approach is to investigate how this aggregate sintering is actually taking place by use of atomistic simulation, and probe how it might differ from the simplest case of binary particles. We use the results to obtain both insight and a better approach to phenomenologically modeling aggregate particle sintering. To the best of our knowledge, there is no MD work that has investigated the sintering of nanoparticle aggregate chains.

In this paper, we focus on the simplest geometric representation of an aggregate, that is, a chain of particles of equal primary particle size. We will use MD simulation to track the evolution of a sintering process and compute the sintering time. We will investigate the applicability or modification to the two-particle sintering model¹¹ for chain aggregates and will present a mathematical model for nanoparticle chain aggregates based on the assumption of viscous flow. We clarify the relationship between chain length and the primary particle size in the dynamics of sintering, provide insight into the relationship between the mathematical model and the MD simulation results, and identify the mechanism of sintering for straight-chain aggregates.

II. MATHEMATICAL MODEL

We begin with the development of a model for coalescence driven by viscous flow. We consider the coalescence of a finite number of particles aligned in a straight chain that are initially in contact with each other [Fig. 1(a)]. We assume that during coalescence, the chain aggregate initially minimizes its surface defects, develops a smooth surface curvature, and forms a columnlike shape [Fig. 1(b)]. Then, the cylinder shrinks axially to minimize its surface area [Fig. 1(c)] and forms an oval shape [Fig. 1(d)]. Finally, the oval

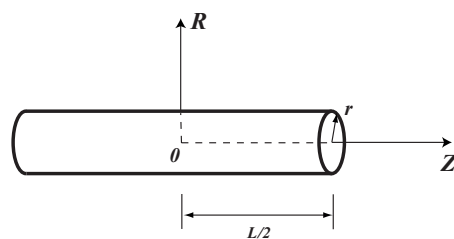


FIG. 2. Geometric representation of a sintering of a rod.

converges to a spherical shape [Fig. 1(e)]. For the coalescence of two particles, the initial (a) and the last (e) steps were investigated by Frenkel¹¹ and by Koch and Friedlander.¹⁸ On the other hand, our chain aggregates are much longer than two particles in contact. Thus, we assume that the steps from (b) to (c) dominate the entire coalescence process of the chain aggregate, and we neglect the initial and final processes from our mathematical model for simplicity.

In the coalescence model, we also assume that the chain aggregate retains its shape as a column during the coalescence (see Fig. 2). From conservation of mass under this condition,

$$\pi r^2 L = \pi (r + \Delta r)^2 (L + \Delta L). \quad (1)$$

The relationship between the change of the radius of the column, Δr , and the change of the length of the column, ΔL , can be obtained as

$$\Delta r = r \left[-\frac{1}{2} \left(\frac{\Delta L}{L} \right) + \frac{1}{8} \left(\frac{\Delta L}{L} \right)^2 + O \left(\left(\frac{\Delta L}{L} \right)^3 \right) \right]. \quad (2)$$

Thus, the radial component of the velocity, u_r , can be approximated as

$$u_r = -\frac{1}{2} \left(\frac{r}{L} \right) u_z, \quad (3)$$

where u_z is an axial component of the velocity. Using Eq. (2), the corresponding surface area change ΔS due to shrinkage of the body is obtained as

$$\Delta S = \pi r \left[1 + \frac{1}{2} \left(\frac{r}{L} \right) \right] (\Delta L) + \text{HOT}. \quad (4)$$

The internal energy, due to the change in surface area S , is related to the surface tension, such that the rate of energy change during the coalescence of the chain aggregates can be expressed as

$$-\sigma \frac{dS}{dt} = -\sigma \pi r \left[1 + \frac{1}{2} \left(\frac{r}{L} \right) \right] \frac{dL}{dt}, \quad (5)$$

where σ denotes the surface tension of the drop. Equation (5) must balance the rate of energy dissipation due to viscous flow of the liquid. The continuity equation of the incompressible flow for an axisymmetric cylindrical coordinate system is given as

$$\frac{\partial u_z}{\partial z} + \frac{u_r}{r} + \frac{\partial u_r}{\partial r} = 0. \quad (6)$$

If the origin of the rod remains fixed, the velocity of any location in the body can be represented by the following equations:

$$u_z = -\alpha z \quad \text{and} \quad u_r = \frac{1}{2}\alpha r, \quad (7)$$

where $\alpha(t)$ is a parameter specifying the velocity gradient. Denoting the length of the column at the instant t with $L(t)$, we have, according to Eq. (7),

$$\frac{dL}{dt} = -\alpha \frac{L}{2}, \quad (8)$$

where $\alpha/2$ is the linear compression coefficient per unit time. The energy dissipated in the whole body per unit time is equal to¹⁹

$$2\eta \int_0^L \int_0^r \left[\left(\frac{\partial u_r}{\partial r} \right)^2 + \left(\frac{u_r}{r} \right)^2 + \left(\frac{\partial u_z}{\partial z} \right)^2 + \left(\frac{\partial u_r}{\partial z} + \frac{\partial u_z}{\partial r} \right)^2 \right] 2\pi r dr dz = 3\eta\alpha^2 \pi r^2 L, \quad (9)$$

where η is the viscosity.

Equating expressions (5), (8), and (9), we obtain the following expression for the velocity gradient parameter α :

$$\alpha = -\frac{\sigma}{3\eta r} \left[1 + \frac{1}{2} \left(\frac{r}{L} \right) \right]. \quad (10)$$

The diffusion coefficient, viscosity, and surface tension are obviously important in coalescence events. At the microscopic level, coalescence is essentially an atomic diffusion process. The surface diffusion coefficient depends on curvature of the particle surface.³ Also, the driving force for coalescence is a minimization of the surface energy. However, based on prior MD calculations where we did not see a significant size dependence on both diffusion coefficient and surface tension for silicon, we use it as a fixed parameter in our phenomenological model.^{20,21} From Eqs. (8) and (10) and integrating over the entire coalescence process, which is the initial chain length L_0 , to $(4V/\pi)^{1/3}$, i.e., when the diameter of the cylinder is equal to the length of the cylinder, where V is the total volume of the column, gives

$$\int_0^t dt = \frac{\eta}{\sigma} \int_{L_0}^{(4V/\pi)^{1/3}} \frac{6}{2\sqrt{\frac{\pi}{V}}L^{3/2} + 1} dL. \quad (11)$$

Thus, the time required for the coalescence of the chain aggregates is given by

$$t = \frac{\eta}{\sigma} \left(\frac{2V}{\pi} \right)^{1/3} (A + B + C), \quad (12)$$

where

$$A = -2\sqrt{3} \left\{ \arctan \left[\frac{1 - 2^{5/3}}{\sqrt{3}} \right] - \arctan \left[\frac{1 - 2(2\sqrt{\pi/V})^{1/3}\sqrt{L_0}}{\sqrt{3}} \right] \right\},$$

$$B = -2 \left\{ \ln[1 + 2^{2/3}] - \ln \left[1 + \left(2\sqrt{\frac{\pi}{V}} \right)^{1/3} \sqrt{L_0} \right] \right\},$$

$$C = \ln[1 - 2^{2/3} + 2^{4/3}] - \ln \left[1 - \left(2\sqrt{\frac{\pi}{V}} \right)^{1/3} \sqrt{L_0} + \left(2\sqrt{\frac{\pi}{V}} \right)^{2/3} L_0 \right].$$

Note that, as we mentioned at the beginning of this section, the model assumes that the coalescence process of chain aggregates follows steps 1(a) through 1(e). The justification of the assumption is based on the MD simulations to be presented later in the text.

III. COMPUTATIONAL MODEL AND NUMERICAL PROCEDURE

To track coalescence, we employ an atomistic simulation approach using classical MD. For this study, we use the SW potential for silicon.²² While similar sets of potential energy functions have also been developed by Tersoff,^{23–26} the SW potential is designed to describe interactions in both solid and liquid forms of silicon. Since most synthesis processes leading to cluster formation occur at high temperature, cluster growth by coalescence is dominated by liquidlike characteristics, and the accuracy of the SW potential increases with increasing particle size or temperature. The SW potential energy is a sum of two- and three-body interactions, and the details of the model and its parameters are given in the literature.²²

All simulations were run on a JVN Linux Cluster running up to eight processors. Atom trajectories were determined by integrating the classical equations of motion using the velocity form of the Verlet algorithm,²⁷ with rescaling of atomic velocities at each time step to achieve temperature control. Time steps of 0.5 fs were typically used to ensure energy conservation, and a Verlet neighbor list with parallel architecture was employed in all the simulations, with a neighbor list renewal every ten steps. The simulations take place in a spherical cavity of 200 nm radius using an elastic boundary condition.

The first step in the equilibration process was to prepare silicon particles of various sizes (500, 1000, 2500, 5000, and 10 000 Si atoms) at 2100 K. After removal of angular momentum, particle temperatures were reduced slowly to 1500 K and equilibrated for 50 ps. For the last step in the preparation process, the simulations were switched to a constant energy calculation for 20 ps. If the average temperature of the particle deviated by more than 10 K over this period, the equilibration process was repeated until the particle temperature deviated by less than 10 K.

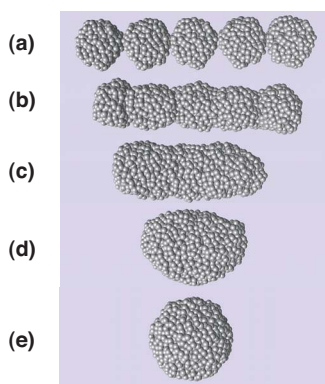


FIG. 3. (Color online) Temporal snapshots of the morphology during sintering of a 5-particle chain aggregate with 500 atoms in a particle at 1500 K.

Duplicated 40 particles were generated and placed on a straight line initially in contact with each other. Since coalescence is an exothermic process, the temperature would increase and affect properties such as diffusivity, which would significantly alter the kinetics. In order to simplify this problem, we chose to study the coalescence process under constant temperature conditions. In fact, for real growth processes, particles of this size would not see temperature excursions since they are effectively thermostated by the surrounding gas.²⁸

IV. RESULTS AND DISCUSSION

A. Short chain aggregates

We begin with a simulation of a short chain aggregate. Figure 3 presents the temporal evolution for an aggregate of five primary particles of 500 Si atoms each aligned in a straight chain. The chain aggregate initially develops a smooth surface curvature and forms a cylinderlike shape [Fig. 3(b)]. The column then shrinks to minimize its surface area and becomes thicker [Fig. 3(c)]. It forms an oval shape [Fig. 3(d)], and finally converges to a spherical shape [Fig. 3(e)]. The above process is the basis from which the phenomenological model in Sec. II was developed. The corresponding structural dynamics for two-, five-, and ten-particle chains can be studied by tracking the temporal variation of the reduced moment of inertia in the direction of collision, and is presented in Fig. 4. The reduced moment of inertia converges to unity when the particle is spherical. However, as these particles are liquidlike, they undergo some thermal fluctuation and therefore would never be truly spherical. Therefore, we define a condition of complete coalescence when the reduced moment of inertia is between 0.9 and 1.1. It can be seen in the figure that for all chain lengths, the reduced moment of inertia converges to 1.1 monotonically. Moreover, the five- and ten-particle chains maintain their initial values of the reduced moment of inertia during the smoothing of its surface [steps (a) and (b)]. We may define this as an induction period, and the period is about 5% of the entire sintering time. Both the sintering time and induction period increase with the increase of the length of the particle

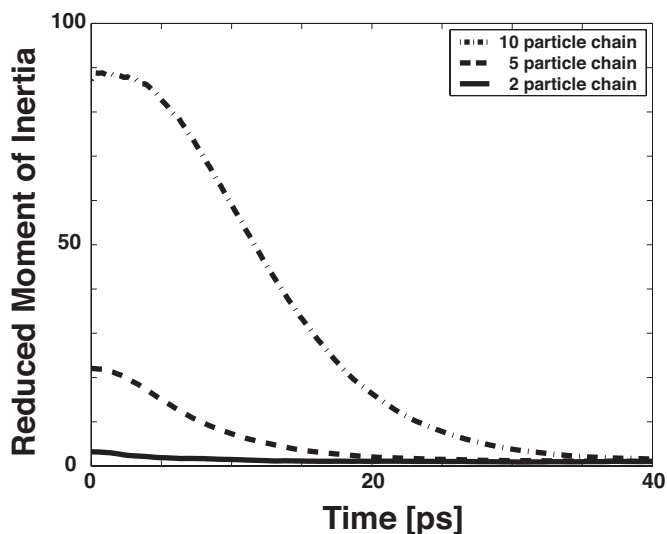


FIG. 4. Temporal behavior of the reduced moment of inertia for 2-, 5-, and 10-particle chain aggregates with 500 atoms in a particle at 1500 K.

chain. Schmid *et al.* (2004) presented a sketch of the evolution of a six-particle chain during sintering. They assumed that the remaining parts of the particle chain maintained a spherical shape, and the shrinkage of the chain was much faster than that obtained from our MD calculations. Moreover, the induction period was never observed in their model.

To better understand the nature of the evolution in the morphology, we study the properties of particle chains in detail. The change in morphology of the clusters could be through movement of atoms via bulk fluid motion or by atomic diffusion processes. Figure 5 shows the temporal evolution of the axial component of the atomic velocity for all atoms in the chain aggregate during sintering. The noise represents the velocity oscillations of ± 50 m/s through the chain. The temporal snapshots show that during the initial

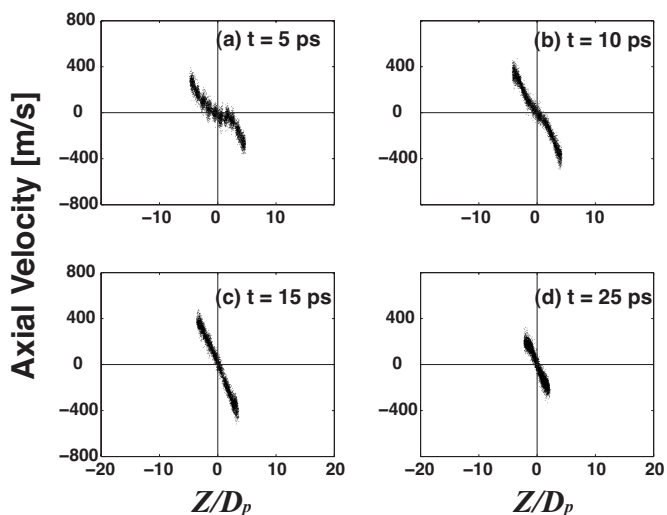


FIG. 5. Time series of axial velocity profile of all atoms in a 10-particle chain aggregate with 500 atoms in a particle at 1500 K. Horizontal axis represents the chain length normalized by the diameter of an initial primary particle.

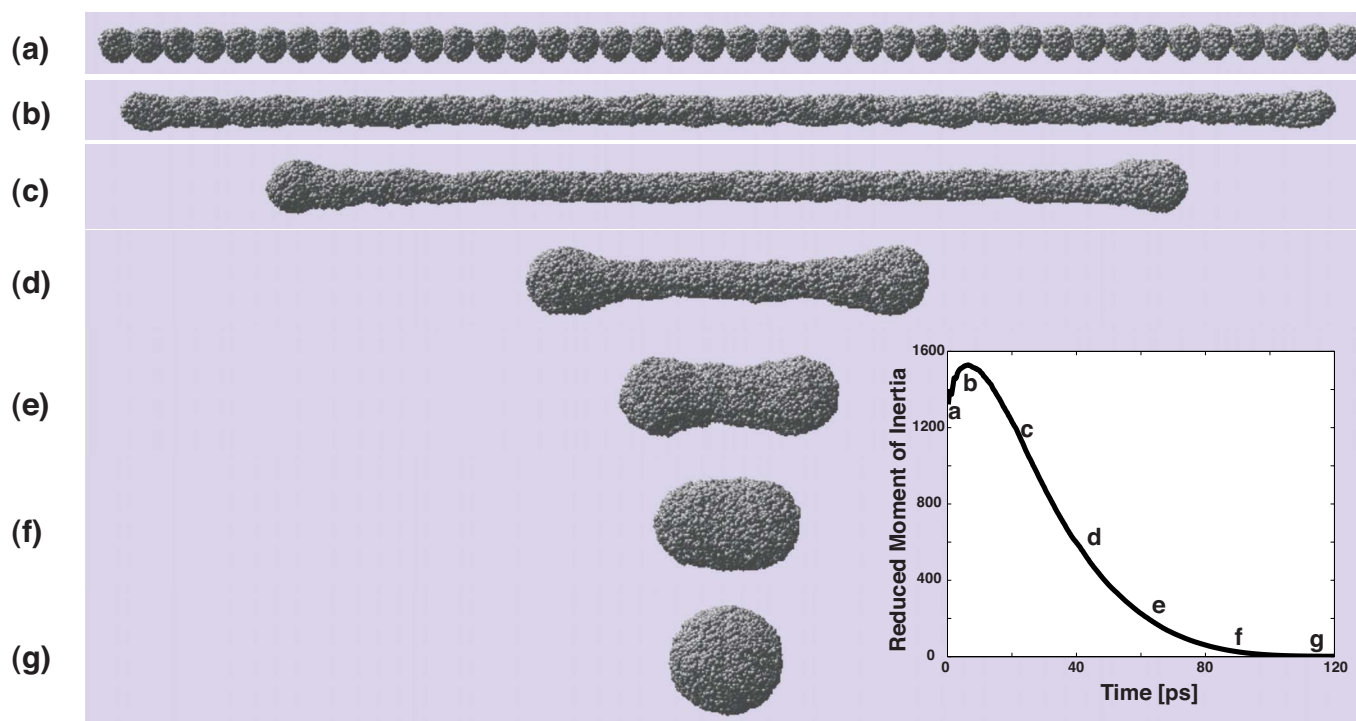


FIG. 6. (Color online) Temporal snapshots of the morphology and corresponding reduced moment of inertia during sintering of a 40-particle chain aggregate with 500 atoms in a particle at 1500 K.

states of sintering, only the ends of the chain have a net velocity, while the rest of the chain is stationary [Fig. 5(a)]. At later times, the velocity gradient becomes linear throughout the chain [Fig. 5(b)] with an increasing gradient in the axial velocity profile with time [Fig. 5(c)].

Note that the linear velocity gradient is predicted from Eq. (7) in the derivation of our phenomenological model. Once a linear velocity profile is developed in the particle chain, the chain length becomes shorter as predicted by the phenomenological model [Fig. 5(d)]. This observation indicates that the sintering process generally follows our phenomenological model subsequent to the initial induction period. More analysis of these results will be presented later in the paper.

B. Long chain aggregates

Figure 6 shows the temporal variation of the particle morphology for a 40-particle chain aggregate of primary particles of 500 Si atoms. The initial behavior is similar to the short chain aggregate; however, as can be seen in Fig. 6(c), as the cylinder begins to shrink, mass accumulates at the ends of the rod in the form of a dumbbell. Basically, what is happening is that atoms in the center of the cylinder are being pulled by neighbors on either axial side, while atoms at the end of the aggregate have neighbors only to one side. So, as the aggregate tries to shrink, it is easier for the end of the rod to grow. The morphological progression to a sphere is presented in the successive images [Figs. 6(e)–6(g)]. Figure 6 shows the corresponding structural dynamics for this case and the temporal evolution of the reduced moment of inertia in the direction of collision. In contrast to the cases of shorter chain aggregates, longer chain aggregates show an initial in-

crease in the moment of inertia and are attributed to a formation of the large masses at both ends of the chain. There have only been a limited number of studies of chain aggregate sintering in the gas phase. Tsyganov *et al.* experimentally studied the sintering of Ni nanoparticle agglomerates in the gas phase.²⁹ They showed a series of transmission electron microscopy micrographs of particle agglomerates which have been sintered for 7 s at temperatures in the range between 300 and 1073 K. They observe that with increasing temperature the necks between the primaries vanish, similar to our observation in Fig. 6(b). A true comparison, however, is not possible since their mechanism of sintering is diffusion controlled and is therefore at an effectively lower temperature. Accessing such a low temperature with MD simulation is prohibitively expensive at this time. Other problems with experimental comparisons are that experiments typically have a range of primary particle sizes within the aggregate, while our prototype aggregate is monodisperse. Our future efforts are aimed at exploring the role of primary particle size distribution on the overall sintering of aggregates.

The corresponding temporal evolution of the atomic velocity of all atoms in the chain aggregate during sintering is shown in Fig. 7. As we have seen in the previous short chain case, sintering progresses first only at both ends [Fig. 7(a)]. The velocity is a maximum for the atoms at the end of the rod and rapidly approaches zero for most of the particle. The maximum velocity is essentially constant until the linear velocity gradient is achieved, at which point the end-atom velocities decrease with time. Once the linear velocity profile is achieved ($L/D_p \sim 10$), a direct observation shows that the decay of the velocity toward a spherical shape is similar to that of the shorter chain case [Figs. 7(c) and 7(d)].

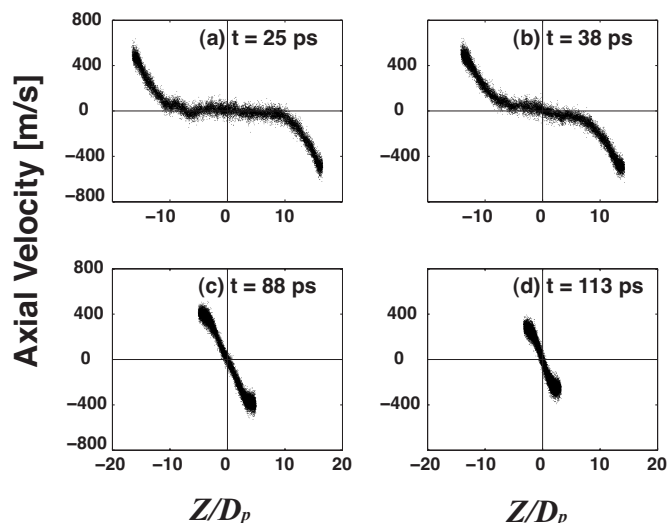


FIG. 7. Time series of axial velocity profile of all atoms in a 40-particle chain aggregate with 500 atoms in a particle at 1500 K. Horizontal axis represents the chain length normalized by the diameter of an initial primary particle.

To understand the role of primary particle size, we can monitor the contraction rate for aggregates of different primary particle sizes. We find that after the initial induction period, which increases with increasing primary particle size, the contraction rate is a constant for any given primary particle size and is independent of chain length. However, the contraction rate is nonlinearly dependent on primary particle size, and as expected small primaries lead to higher contraction rates. We summarize the role of primary particle size, as represented by the cubic root of the number of atoms (proportional to diameter) in a primary particle in Fig. 8. The maximum contraction rate v in m/s can be described by

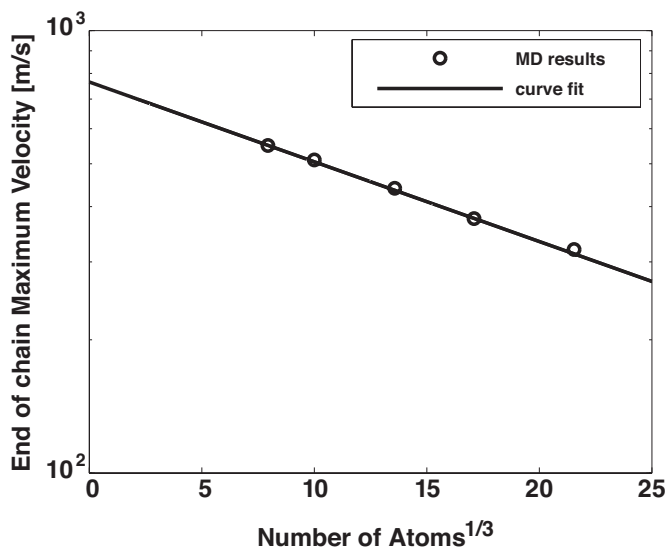


FIG. 8. End-of-chain maximum velocity as a function of the size of a particle.

$$v = 765e^{-0.042N^{1/3}}, \quad (13)$$

where N is the number of atoms in a primary particle. This result is used in our later comparison to the phenomenological model.

C. Comparison of phenomenological model with MD results

The MD simulations show that sintering of particle chain aggregates consists of three steps. Step (a) is coalescence between particles to develop a rodlike shape. Step (b) is contraction of the column structure, which actually consists of two different contraction stages. The first stage is the local contraction stage where sintering occurs only at the ends of the particle chain, and the second stage is where the global contraction takes place and is the focus of the phenomenological model we developed. Step (c) is the nominal sintering process from an oval to spherical shape, which can be seen in any sintering process independent of initial structure of the particle chain aggregates. In the derivation of the phenomenological model, we neglected both steps (a) and (c) because we assumed that the particle chain is sufficiently long so that step (b) dominates the entire sintering process. However, the model, which is derived based on the assumption of continuum and viscous flow, cannot predict the local sintering process that induces the nonlinear velocity profile (or the discontinuity in the velocity gradient) in the axial direction that occurs in the first stage of the second step (see Fig. 7). The velocity gradient α in Eqs. (7) and (10), which is a function of time, suggests that the mobility of all atoms in the particle chain depends on the location of the atom, the length of the chain, and the size of the primary particle. The expression for u_z [Eq. (7)] suggests that the maximum contraction speed for an aggregate occurs at the end of the chain and depends linearly on the length of the chain at any time during sintering. This behavior is in contrast to the isotropic contraction predicted by the viscous flow model (Fig. 7) and points to the limitation of the model.

The above discussion indicates that in order to accurately capture the dynamics of sintering, the present phenomenological model will require that the initial conditions for the velocity profile be used from the MD simulations. Figure 9 shows the temporal variation of the end-of-chain velocity for various chain lengths, 10-, 40-, and 40-particle chains with 500, 500, and 5000 atoms per primary particle. The initial axial velocity is independent of the particle chain length, at fixed primary particle size, and only deviates moderately at the later stages of sintering. When primary particle size is larger, both the initial velocity and the initial linear acceleration are lower due to the lower surface to volume ratio to move atoms.

For primary particle sizes from 500 to 10 000 atoms, the initial edge velocity [Eq. (14)] and the initial edge acceleration [Eq. (15)] can be fitted quite well.

$$v_i = 604e^{-0.209N^{1/3}}. \quad (14)$$

The acceleration, however, is best fitted to the particle volume and approximated as

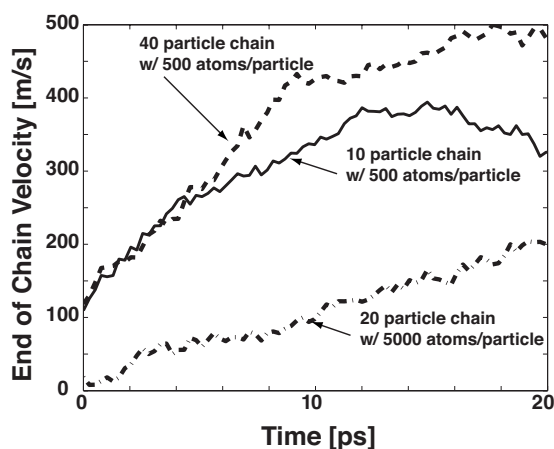


FIG. 9. Temporal change of end-of-chain axial velocity during the initial sintering process for various chain cases, 10-, 40-, and 40-particle chain with 500, 500, and 5000 atoms per primary particle.

$$a_i = 0.36e^{-0.000277N}, \quad (15)$$

where v_i is the axial component of the initial edge velocity in m/s and a_i is the initial edge acceleration in $\text{\AA}/\text{ps}^2$. We note that the initial velocity scales with diameter, while acceleration scales with primary particle volume.

In order to capture the dynamics of sintering of nanoparticle chain aggregates, in our viscous flow phenomenological model we apply the initial conditions obtained from MD simulations [Eqs. (13) and (14)] to the viscous flow model [Eq. (12)]. We use the initial velocity and linear acceleration conditions [Eqs. (14) and (15)] until the end-of-chain speed reaches the maximum speed found from Eq. (13). Then, the contraction rate is held constant until the velocity profile becomes linear.

A comparison of the viscous flow model and the MD simulations for the sintering times for various chain and primary particle sizes is summarized in Fig. 10. For these evaluations, and in accordance to our prior simulations, the surface tension of silicon nanoparticles was size independent, i.e., curvature independent.²¹ Thus, we applied the surface tension values obtained from the nanoparticle simulations for the present rodlike structures. The surface tension σ was taken as 0.826 J/m^2 , as computed by our prior simulations. The viscosity η of 5.9 cP was chosen to fit the MD results. By comparing this suggested value with the experimental data of bulk liquid silicon viscosity, which is 0.88 cP at 1690 K ,³⁰ we found a factor of 7 discrepancy with the bulk experimental data. It is known that viscosities for liquids cannot be well estimated theoretically. Moreover, liquid viscosities are affected drastically by temperature and melting point of the medium, and the melting point also strongly depends on the size of nanoparticles. Thus, the value of diffusion coefficient found in our prior silicon nanoparticle simulation is also applied to the expression for a relationship between diffusion coefficient and bulk viscosity obtained by Glasstone *et al.*,³¹

$$\eta = kT/a_0D_0, \quad (16)$$

where k and a_0 are the Boltzmann constant and the distance between atoms, respectively. The value of a_0 is selected to be

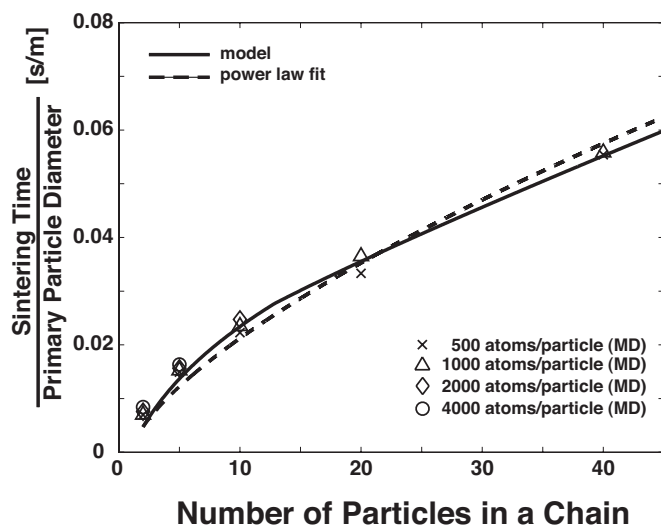


FIG. 10. Sintering times per primary particle diameter vs as number of particles in a chain, for 500, 1000, 2000, and 4000 atoms/particle. Symbols, MD results; solid line, model; dashed line, power law curve fit.

2.352 \AA , which corresponds to the covalent-bond distance, and the value of D_0 is selected to be $4.5 \times 10^{-5} \text{ cm}^2/\text{s}$ from the prior simulation. The calculated value of the bulk viscosity is 19.6 cP , which is about three times larger than the value we estimated. This comparison also does not show excellent agreement; however, the diffusion coefficient computed from the SW potential showed agreement with those of tight-binding molecular dynamics,³² and the SW potential is designed to describe the melting phase of silicon. Because of the uncertainties in property values, a direct quantitative comparison between the viscous flow model and the MD simulation gives a sintering from MD that is a factor of 3 faster, which we can use as a universal calibration constant, $\kappa = 0.3$. If we consider that the surface tension determined by MD is quite accurate, this factor κ can be considered to be a correction to the viscosity. We use this value only as a correction factor to the viscous flow model to aid in comparison.

We plot the MD simulated sintering time of the chain normalized by primary particle diameter vs the number of primary particles in the chain for 500, 1000, 2000, and 4000 atoms per primary particle in Fig. 10. The choice of plotting the MD results in terms of a normalized sintering time is based on our phenomenological model sintering time, expressed in Eq. (12), which shows a linear dependence on diameter. The data points correspond to the MD simulations and indicate a monotonic increase in sintering time with increasing chain length or primary particle diameter for all sizes of primary particles. By plotting the normalized sintering time, we obtain results that are independent of primary particle diameter and only depend on the number of primary units. A comparison with the phenomenological model for the case of 500 atoms/particle is shown as a solid line in the figure. Our model (scaled by $\kappa = 0.3$) shows excellent agreement for all lengths and sizes of chain aggregates. Moreover, the model accurately captures the transition of the sintering time to a linear dependence on chain length for

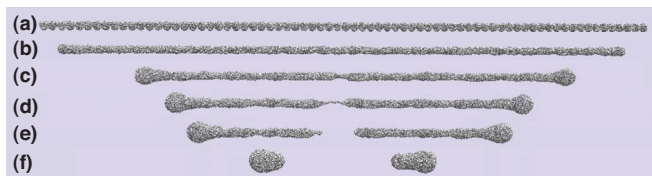


FIG. 11. (Color online) Temporal snapshots of the morphology during sintering of a 73-particle chain aggregate with 500 atoms in a particle at 1500 K.

aggregates with more than 10 primaries. This occurs because the maximum end-of-chain speed is achieved and the constant contraction rate is established for long chain lengths. The viscous flow model despite its obvious limitation, particularly with regard to the isotropic sintering assumption, correctly captures the primary particle size dependence and the chain length dependence on the sintering time, thus indicating that the flow even at these length scales can reasonably be modeled with a continuum representation.

The nature of the data presented in Fig. 10 presents the opportunity to provide a power law relationship amenable to application to phenomenological sintering models. Our model [Eq. (12)] and its comparison with the MD simulation indicate that the sintering follows a viscous flow route. For viscous flow, Frenkel gave the coalescence time for the two particles of equivalent size by

$$t_{\text{Frenkel}} = \frac{4\eta r_0}{3\sigma}, \quad (17)$$

where r_0 denotes the initial radius of a sintering particle. This model considers the coalescence of two liquid drops, which are initially in contact with each other at a single point. The model also assumes that the remaining parts of the two drops maintain a spherical shape. Under this condition, the distance between the centers of each drop is equal to $2r_0 \cos \theta$. From conservation of mass of each drop, the relationship between the radius r_0 and the total surface of the coalescing particles at any time t and at $t=0$, and from conservation of energy of surface tension and viscous dissipation of coalescing drops, the Frenkel expression [Eq. (17)] can be obtained.¹¹ Thus, we approximate the coalescence time for chain aggregate nanoparticles as a modification of the Frenkel model by

$$t_c = t_{\text{Frenkel}}(N-1)^m, \quad (18)$$

where N is the number of the particles in a chain and m is a power constant fit to the results presented in Fig. 10, which yields a result of $m=0.68$. The comparison as presented in Fig. 10 indicates that this fit provides a convenient way to incorporate aggregate sintering into an aerosol model.

D. Very long chain aggregates

For all the simulations discussed above, we always observed sintering of the chain aggregate. However, we have noticed that if the chain contained a large number of primaries, the chain would fragment. Figure 11 presents an example of a 73-nanoparticle chain of 500 atoms/particle. The initial process is similar to the long chain case [Figs. 11(a)

and 11(b)]. However, while the cylinder begins to shrink and mass accumulates at the ends of the cylinder, the cross-sectional area of the central region of the cylinder begins to decrease due to a local instability [Fig. 11(c)]. In the traditional mechanics community, this type of behavior in a macroscopic material during, for example, a tensile measurement is known as necking. The local instability quickly diminishes its cross-sectional area and elongates the middle portion of the cylinder [Fig. 11(d)]. The chain finally ruptures [Fig. 11(e)], and each fragment sinters independently into two spherical particles [Fig. 11(f)]. The driving force for sintering is the minimization of surface area, and the strength of the driving force is proportional to the surface area of the chain aggregate. For straight chain aggregates, the surface area is proportional to the number of particles contained in the chain. Thus, for a chain with a large number of primaries, the normal stress induced by the surface energy exceeds its critical value, and the particle chain aggregate cannot support its long shape and breaks so as to reduce its surface energy below its critical value for each resulting chain. The critical value may depend on its chain length (surface energy), primary particle size (stress), and temperature (diffusivity) of the system. Further investigations are beyond the scope of this paper.

V. CONCLUSION

MD simulation is used to investigate the sintering of silicon nanoparticle straight-chain aggregates. We considered particle chain lengths up to 80 and primary particles of 2.5 (500 atoms/particle) to 7 nm (10 000 atoms/particle) in diameter. We found that sintering of chain aggregates consists of three steps. In step (a), reaction between particles to minimize surface defects and development of a cylindrical like shape comprised an induction period. Step (b) consisted of contraction of the cylinder, which actually consisted of two contraction stages. The first stage was the local contraction stage, where sintering occurs only at the ends of the particle chain, and the second stage involved the global contraction. The last step is the nominal sintering process from an oval to spherical shape. As expected, sintering time increases with increasing chain length. The sintering times normalized by the primary particle diameter showed a universal relationship which only depends on chain length. These results were found to be consistent with a mathematical model based on continuum viscous flow. The model was able to predict the sintering time with excellent agreement with the results obtained from molecular dynamics for any chain length and any primary particle size for a straight nanoparticle chain aggregates. The results¹⁵ for sintering times for aggregate chains could be summarized with a power law modification of the Frenkel viscous flow equation, which depends on the number of particle connections in a chain aggregate.

ACKNOWLEDGMENTS

Support for this work comes from the National Science Foundation and the National Institute of Standards and Technology.

*Corresponding author; mrz@umd.edu

- ¹J. H. Helble and A. F. Sarofim, *J. Colloid Interface Sci.* **128**, 348 (1989).
- ²M. D. Barnes, S. M. Mahurin, A. Mehta, B. G. Sumpter, and D. W. Noid, *Phys. Rev. Lett.* **88**, 015508 (2002).
- ³Y. Xing and D. E. Rosner, *J. Nanopart. Res.* **2**, 277 (1999).
- ⁴V. L. Colvin, A. P. Alivisatos, and J. G. Tobin, *Phys. Rev. Lett.* **66**, 2786 (1991).
- ⁵A. N. Goldstein, C. M. Echer, and A. P. Alivisatos, *Science* **256**, 1425 (1992).
- ⁶A. P. Alivisatos, *Science* **271**, 933 (1996).
- ⁷J. Shi, S. Gider, K. Babcock, and D. D. Awschalom, *Science* **271**, 937 (1996).
- ⁸F. E. Kruijs, H. Fissan, and A. Peled, *J. Aerosol Sci.* **29**, 511 (1998).
- ⁹C. Artelt, H. J. Schmid, and W. Peukert, *J. Aerosol Sci.* **36**, 147 (2004).
- ¹⁰S. K. Friedlander and M. K. Wu, *Phys. Rev. B* **49**, 3622 (1994).
- ¹¹J. Frenkel, *J. Phys. (Moscow)* **9**, 385 (1945).
- ¹²M. R. Zachariah and M. J. Carrier, *J. Aerosol Sci.* **30**, 1139 (1999).
- ¹³T. Hawa and M. R. Zachariah, *Phys. Rev. B* **71**, 165434 (2005).
- ¹⁴T. Hawa and M. R. Zachariah, *J. Aerosol Sci.* **37**, 1 (2006).
- ¹⁵M. K. Akhtar, G. G. Lipscomb, and S. E. Pratsinis, *Aerosol Science and Technology* **21**, 83 (1994).
- ¹⁶P. Kulkarni and P. Biswas, *J. Nanopart. Res.* **5**, 259 (2003).
- ¹⁷H. J. Schmid, S. Tejwani, C. Artelt, and W. Peukert, *J. Nanopart. Res.* **6**, 613 (2004).
- ¹⁸W. Koch and S. K. Friedlander, *J. Colloid Interface Sci.* **140**, 419 (1990).
- ¹⁹G. K. Batchelor, *An Introduction to Fluid Dynamics* (University Press, Cambridge, 1967).
- ²⁰M. R. Zachariah, M. J. Carrier, and E. Blaisten-Barojas, *J. Phys. Chem.* **100**, 14856 (1996).
- ²¹T. Hawa and M. R. Zachariah, *J. Chem. Phys.* **121**, 9043 (2004).
- ²²F. H. Stillinger and T. A. Weber, *Phys. Rev. B* **31**, 5262 (1985).
- ²³J. Tersoff, *Phys. Rev. Lett.* **56**, 632 (1986).
- ²⁴J. Tersoff, *Phys. Rev. B* **37**, 6991 (1988).
- ²⁵J. Tersoff, *Phys. Rev. B* **38**, 9902 (1988).
- ²⁶J. Tersoff, *Phys. Rev. B* **39**, 5566 (1989).
- ²⁷L. Verlet, *Phys. Rev.* **159**, 98 (1967).
- ²⁸D. Mukherjee, C. G. Sonwane, and M. R. Zachariah, *J. Chem. Phys.* **119**, 3391 (2003).
- ²⁹S. Tsyganov, J. Kastner, B. Rellinghaus, T. Kauffeldt, F. Westerhoff, and D. Wolf, *Phys. Rev. B* **75**, 045421 (2007).
- ³⁰V. M. Glazov, S. N. Chizhevskaya, and N. N. Clagoleva, *Liquid Semiconductors* (Plenum, New York, 1969).
- ³¹S. Glasstone, K. J. Laidler, and H. Eyring, *The Theory of Rate Processes* (McGraw-Hill, New York, 1941).
- ³²C. Z. Wang, C. T. Chan, and K. M. Ho, *Phys. Rev. B* **45**, 12227 (1992).